Catalysis Today 164 (2011) 190–197

Contents lists available at ScienceDirect

Catalysis Today

journal homepage: www.elsevier.com/locate/cattod

Hydrogen generation from *n*-tetradecane, low-sulfur and Fischer–Tropsch diesel over Rh supported on alumina doped with ceria/lanthana

Xanthias Karatzas[a,*], Derek Creaser[b,c], Ann Grant[c], Jazaer Dawody[d], Lars J. Pettersson[a]

[a] KTH – Royal Institute of Technology, Department of Chemical Engineering and Technology, Teknikringen 42, SE-100 44 Stockholm, Sweden
[b] Chalmers University of Technology, Chemical Reaction Engineering, SE-412 96 Göteborg, Sweden
[c] Volvo Technology Corporation, Chalmers Science Park, SE-412 88 Göteborg, Sweden
[d] PowerCell Sweden AB, Ruskvädersgatan 12, SE-418 34 Göteborg, Sweden

ARTICLE INFO

Article history:
Available online 5 November 2010

Keywords:
Autothermal reforming
Ceria
Cordierite monolith
Diesel
Lanthana
Rhodium

ABSTRACT

The present study demonstrates the use of rhodium-based monolithic catalyst for onboard reforming of diesel fuels. Experimental results from hydrogen generation of *n*-tetradecane, low-sulfur and Fischer–Tropsch diesel, via autothermal reforming (ATR), were acquired with a catalyst consisting of 3 wt% Rh supported on alumina doped with Ce/La. The catalyst was prepared by impregnation using the incipient wetness technique, and deposited onto a 400 cpsi cordierite monolith. Furthermore, the catalyst was tested over ranges of oxygen-to-carbon and water-to-carbon feed ratios, both in a bench-scale and a full-scale reactor. Fresh powder samples of the catalyst were characterized by XRD, N_2-BET, H_2 chemisorption, H_2-TPR and XPS analyses.

The activity results showed that high fuel conversions and hydrogen production could be achieved with 3 wt% Rh for all fuels. Furthermore, the highest formation of CO and C_2H_4 was found in the product gas stream from the low-sulfur diesel. In addition, partial oxidation and steam reforming reactions were identified by closely studying the distribution of the analyzed product gas composition and the temperature measurements.

The characterization results showed the presence of finely dispersed Rh particles in the support. Furthermore, bulk and surface rhodium oxides were detected, which have been suggested to be one of the major active phases for ATR of diesel. Bulk and surface cerium oxides (CeO_2) and surface La in the dispersed phase were also found to be present in the catalyst composition. These promoters are believed to improve the catalyst activity and durability.

1. Introduction

Fuel-cell auxiliary power units (FC-APU) and hydrocarbon selective catalytic reduction (HC-SCR) are being proposed as two major strategies for introducing hydrogen in the transport sector to reduce emissions [1–4]. Heavy-duty truck APUs are used to provide electricity to the vehicle at standstill to reduce idling emissions, while HC-SCR units are employed for reduction of NO_x at lean engine operation. Catalytic onboard reforming technologies are considered feasible alternatives for supplying these units with hydrogen by using the existing truck fuel. Autothermal reforming (ATR) has received considerable attention lately as one of the most promising methods for generating hydrogen from diesel. In this work, the performance of ATR-catalysts, using engineered substrates in the form of wash-coated monoliths, was studied for realistic application conditions. Diesel surrogate, *n*-tetradecane, and commercial low-sulfur and Fischer–Tropsch diesel fuels were tested in order to provide a deeper understanding regarding the role of the fuel properties and possible reaction mechanisms. Previous work in our laboratory has demonstrated an industrial-scale diesel reformer capable of providing low fuel slip and high production of hydrogen [5,6]. The same reactor system, with the inclusion of new in-house made Rh-based monolithic catalysts, has been used in this study.

In this study, ATR and steam reforming (SR) of low sulfur diesel was tested at bench scale to detect differences in activity for a catalyst consisting of 3 wt% Rh supported on δ-alumina doped with Ce/La. The catalyst performance and stability was also tested in an industrial scale reactor whose capability has been demonstrated with excellent results in an earlier work [5,6]. The catalyst was tested over ranges of oxygen-to-carbon and water-to-carbon feed ratios using *n*-tetradecane, and commercial low-sulfur and Fischer–Tropsch diesel. Finally, fresh powder samples of the cata-

* Corresponding author. Tel.: +46 87909150.
E-mail address: xanthias@ket.kth.se (X. Karatzas).

0920-5861/$ – see front matter © 2010 Elsevier B.V. All rights reserved.
doi:10.1016/j.cattod.2010.10.019

Table 1
Washcoat properties for the alumina support and catalyst used in this study. The surface area and porosity were measured by N_2-BET, the dispersion and crystallite size of Rh were determined by H_2 chemisorption, while the crystallite size of ceria was determined by XRD.

Sample	Surface area (m^2/g)	Pore volume (cm^3/g)	Pore diameter (Å)	H/Rh (%)	d_p (Rh) (nm)	$d_p(CeO_2)$ (nm)
δ-Al_2O_3	105	0.92	349	–	–	–
$Rh_{3.0}Ce_{10}La_{10}$/δ-Al_2O_3[a]	80	0.43	185	42	2.6	8.1

[a] The first three subscripted values reveal the nominal weight loading of the active metal and promoters on the support.

lyst were characterized by XRD, N_2-BET, H_2 chemisorption, H_2-TPR and XPS analyses.

2. Experimental

2.1. Catalyst preparation

Table 1 exhibits the washcoat properties of the Rh-based catalyst used in this study. The metal precursors used for the catalyst preparation were Rh nitrate ($Rh(NO_3)_3$, Rh 8–10% w/w, Sigma Aldrich), Ce nitrate ($Ce(NO_3)_3{\cdot}6H_2O$, 99.99%, Alfa Aesar) and La nitrate ($La(NO_3)_3{\cdot}6H_2O$, 99.9%, Alfa Aesar) solutions. The δ-alumina was made by calcining γ-alumina (PURALOX HP-14/150, Sasol Germany GmbH) at 1000 °C for 1 h. The alumina powder was impregnated with the metals by the incipient wetness (IW) technique in accordance to the weight loading presented in Table 1. The resulting powders were calcined at 800 °C for 3 h and deposited via the ethanol-slurry dip-coating procedure onto 400 cpsi cordierite monoliths (Corning). For the bench-scale test, monoliths with dimensions OD = 17.8 mm, l = 30.5 mm were used. For the full scale test, two monoliths with dimensions OD = 80.3 mm, l = 76.2 mm covered with the same washcoat were used.

2.2. Characterization

In this study only fresh catalyst powder was characterized. The powder was taken from the preparation procedure prior to deposition on the cordierite monoliths. The fresh catalyst powder was characterized by the following techniques:

- Surface area and pore size distribution were measured by nitrogen adsorption at liquid N_2 temperature using a Micromeritics ASAP 2010 instrument. Prior to analysis the catalyst powder, ~0.4 g, was degassed at 250 °C.
- The crystal phases were determined by X-ray diffraction (XRD), using a Siemens Diffraktometer D5000 scanning 2θ from 10° to 90° in the scan mode (0.02°, 1 s), using Ni filtered Cu Kα radiation.
- Temperature programmed reduction (TPR) was performed with hydrogen using a Micromeritics Autochem 2910 equipped with a thermal conductivity detector (TCD). Approximately 0.1 g of catalyst powder was used for each analysis. The sample was reduced with 5 vol% H_2 in Ar (50 cm^3/min) using a heating rate of 10 °C/min from room temperature to 1000 °C.
- The dispersion and the crystallite size of the Rh particles were measured by hydrogen chemisorption analysis, using a Micromeritics ASAP 2020. The sample, ~0.2 g, was pre-reduced by hydrogen at a temperature set to 600 °C, helium treated at 450 °C and finally hydrogen treated and analyzed at 40 °C. The atomic stoichiometric value of H/Rh = 1 was used for processing of the chemisorption data.
- The surface composition and chemical state of the deposited additives and loaded active metals were determined using X-ray photoelectron spectroscopy (XPS). The XPS studies were performed in a Phi Quantum 2000 system.

2.3. Low-sulfur diesel reforming: bench-scale

The diesel reforming experiments at bench-scale were carried out at a reactor inlet temperature of 650 °C, GHSV ~ 17,700 h^{-1} and P = 1 atm. A standard diesel fuel (6 ppm S, C/H = 6.43) whose physical and chemical properties are in close correlation to Swedish Environmental Class 1 diesel (MK 1) (see Table 2), was used as feedstock. Three reaction conditions were tested; two ATR and one SR. The following operating parameters were employed: H_2O/C = 2.5, O_2/C = 0.49 (λ = 0.33); H_2O/C = 3.0, O_2/C = 0.49 (λ = 0.33); and H_2O/C = 3.0. The experiments were carried out in a vertically mounted stainless steel tubular reactor with ID = 23.7 mm equipped with a heating coil and three thermocouples to control the reactor and feed temperature. The product gases were analyzed using a Gasmet Cr-200 Fourier transform infrared spectrometer (FTIR) and a Maihak modular system S710 equipped with a non-dispersive infrared sensor (NDIR) and TCD.

2.4. Tetradecane, low-sulfur and FT diesel reforming: full-scale

ATR experiments were carried out using n-tetradecane (TCI Europe), commercial Swedish Environmental Class 1 diesel (MK1) (Shell) and Fischer–Tropsch diesel (FramTidsbränslen AB) as feedstocks (see Table 2) at atmospheric pressure. The reaction conditions tested are listed in Table 3. The fuel flow was kept constant at 19.0 g/min for all fuels, resulting in a thermal power input in the range of 13.5–14.0 kW_{th}. The fuels were injected through a stainless-steel spray nozzle (0.23 mm orifice diameter, MistJet®, STEINEN) and blended with a 300 °C preheated air-steam mixture to enable adiabatic operation. The reactions took place inside a horizontally mounted stainless steel tubular reactor with dimensions ID = 84 mm and l = 400 mm. An alumina foam disc (RQ-3085, Selee Corp.) and two monoliths, hereby referred to as CAT1 and CAT2, covered with the same washcoat composition, $Rh_{3.0}Ce_{10}La_{10}$/δ-Al_2O_3, were placed inside the reactor in sequential order. A total of 14 K-type thermocouples (Pentronic) were placed in different locations inside the reactor for temperature measurements. Four of these were placed inside the monoliths at reactor l = 180 and

Table 2
Comparison of properties for the fuels used in this study [7–10].

	n-Tetradecane	Diesel MK1	FT-diesel
Chemical formula	$C_{14}H_{30}$	~$C_{14}H_{26}$	~$C_{14}H_{26}$
Molecular weight (g/mol)	198.4	~194	~194
Boiling point @ 1 bar (°C)	253	180–290[a]	350[a]
Vapor pressure @ 38 °C (bar)	Negl. (20 °C)	Negl.	Negl.
Liquid density @ 15 °C (kg/m^3)	760	800–820	800
Liquid viscosity @ 40 °C (mPa s)	1.7	2–4 (25 °C)	~2.9
Heat of vaporization (MJ/kg)	0.25	0.27	–
Lower heating value (MJ/kg)	44	43	43
Autoignition temperature (°C)	220	206[b]	–
Flammability limits in air (vol%)	0.5–6.5	1–5	–
Sulfur content max (wt ppm)	–	10	2
Aromatic content max (vol%)	–	5	2
Cetane number min (n-cetane)	93	50	80

[a] T95.
[b] n-Cetane.

Table 3
Operating parameters for the fuels used in the full-scale ATR experiments.

Fuel	Flow rate (g fuel/min)	P^{a} (kW_{th})	P_e[b] (kW_e)	O_2/C (mol mol)	λ[c]	H_2O/C (mol mol)	GHSV[d] (h^{-1})
n-Tetradecane	19.0	14.0	5.0	0.37–0.51	0.30–0.33	2.0/2.5/3.2	9300–12,400
Diesel MK1	19.0	13.5	5.0	0.37–0.50	0.29–0.33	2.0/2.5/3.0	9500–12,400
FT diesel	19.0	13.7	5.0	0.39–0.40	0.25–0.26	2.5/3.2	10,200–11,100

[a] Thermal power output.
[b] Electrical power output estimated for an APU system based on Polymer Electrolyte Fuel Cell (PEFC) technology.
[c] Actual-to-stoichiometric air/fuel ratio.
[d] Total GHSV measured for both catalysts in the reactor.

290 mm, respectively, for in situ temperature measurements. In this study, the O_2/C ratio was varied to establish an in situ temperature ranging from 600 to 800 °C for both catalysts. Furthermore, gas samples were taken from the outlets of each monolith. The product gases were analyzed using gas chromatography (GC, Varian CP-3800) and an FTIR (MKS Multigas^{TM} 2030 HS).

During the full-scale ATR experiments *n*-tetradecane was tested first, followed by FT-diesel and diesel MK1. The same pair of catalysts was used for each fuel and the reaction conditions were tested twice to detect any difference in activity. The experiments were run until stable and reproducible results were obtained. During shutdown of the reformer, the air was shut off first, followed by fuel and steam. Air was then flushed through the reformer to burn off potential coke and sulfur deposits on the catalyst surface. Coke and sulfur oxides could then be detected by increases in temperature in the reactor system and by observing the FTIR concentrations of H_2O, CO, CO_2 and SO_2 in the outlet gas. An ocular inspection of the reforming catalysts was also performed after each experiment. Further details concerning the experimental procedure can be found elsewhere [5,6].

3. Results and discussion

3.1. Catalyst characterization

3.1.1. N_2-BET

The results from the porosity measurements of $Rh_{3.0}Ce_{10}La_{10}/\delta$-$Al_2O_3$ using nitrogen-adsorption at liquid N_2-temperature are presented in Table 1. As seen in Table 1, the addition of the active metal and promoters reduced the surface area, pore volume and pore diameter of the alumina support. For instance, the BET surface area was reduced from 105 to 80 m^2/g while the pore volume was reduced by half.

3.1.2. H_2 chemisorption

The results from the chemisorption measurements are presented in Table 1. High rhodium dispersion ~42% is noted for the catalyst sample indicating that a high number of surface and bulk rhodium atoms were available for hydrogen chemisorption. Furthermore, the addition of ceria did not change the rhodium dispersion while lanthana had a slightly negative effect, as demonstrated in previous work [6].

3.1.3. X-ray diffraction

Diffraction peaks associated with the phases in the alumina-supported catalyst $Rh_{3.0}Ce_{10}La_{10}/\delta$-$Al_2O_3$ are labeled in Fig. 1. The XRD pattern of the fresh catalyst powder shows that the δ-phase of alumina is present [11]. Furthermore, the peaks at $2\theta = 28.5°$, 48.5° and 56.5° are ascribed to fluorite-structured CeO_2 [12]. The average crystallite size of ceria was ~8.1 nm (see Table 1), calculated by the Scherrer equation at $2\theta = 28.5°$, hence indicating that the particles are well dispersed in the support. The addition of lanthana did not reveal any other phases than δ-Al_2O_3 and CeO_2. However,

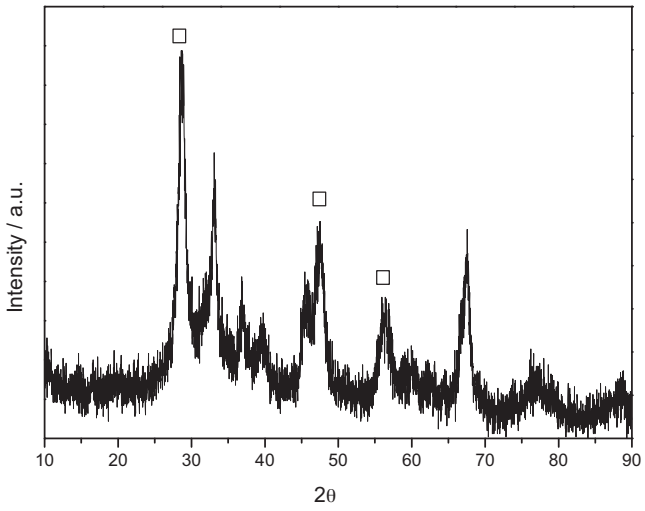

Fig. 1. XRD patterns for 2θ between 10° and 90° at room temperature of $Rh_{3.0}Ce_{10}La_{10}/\delta$-$Al_2O_3$. Reflections of (□) fluorite-structured CeO_2.

it was found that lanthana lowered the intensity of the diffraction peaks and enhanced the ceria dispersion [6]. Rhodium phases were not detected by XRD, indicating that the rhodium particles are small and well dispersed in the washcoat. This observation was confirmed by hydrogen chemisorption analysis as the Rh crystallite size was ~2.6 nm, see Table 1.

3.1.4. Temperature-programmed reduction

The TPR profile of $Rh_{3.0}Ce_{10}La_{10}/\delta$-$Al_2O_3$ is shown in Fig. 2. The reduction peak present at 150 °C can be ascribed to reduction of bulk rhodium oxides species RhO_x, see Eq. (1) [13], the peak at

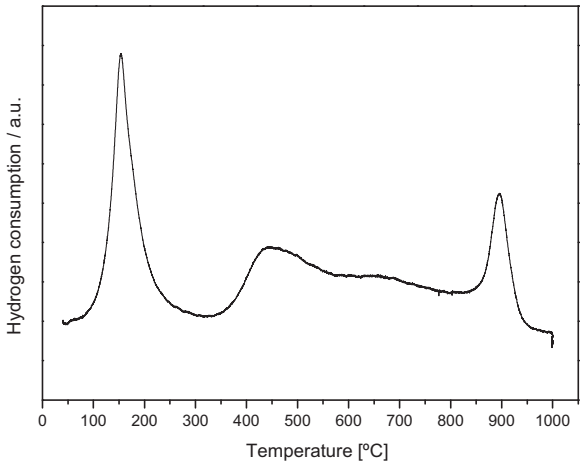

Fig. 2. TPR profile of $Rh_{3.0}Ce_{10}La_{10}/\delta$-$Al_2O_3$. The hydrogen consumption is displayed as function of temperature.

Table 4
Binding energies and surface atomic ratios for fresh powder sample $Rh_{3.0}Ce_{10}La_{10}/\delta$-$Al_2O_3$.

Rh $3d_{5/2}$ (eV)	Ce $3d_{5/2}$ (eV)	La $3d_{5/2}$ (eV)	Rh/Al	Ce/Al	La/Al
308.8	881.8	834.2	0.031	0.008	0.091

450 °C is due to hydrogen spillover onto the alumina support [13] while the peak at 900 °C is attributed to reduction of bulk and surface cerium oxides [14]. Furthermore, it was found that the addition of ceria improved the hydrogen uptake of the RhO_x while the addition of lanthana enhanced the ceria reducibility in the support. Lanthanum oxides were not detected by TPR [6].

$$RhO_x + xH_2 \rightarrow Rh + xH_2O \quad (1)$$

3.1.5. X-ray photon spectroscopy

XPS measurements provided valuable information about the surface composition and oxidation state of the fresh catalyst powder. As seen in Table 4 most elements were found in the oxidized state. Rhodium was found to be present in its oxidized state, possibly in the form of Rh_2O_3 with a binding energy of 308.8 eV [15]. Hence, rhodium oxide species are present on the surface as well as in the bulk as previously discussed in Section 3.1.4. For ceria, the binding energy of the Ce $3d_{5/2}$ line is found at 881.8 eV, indicating CeO_2 [15–17]. Hence, CeO_2 species are present on the surface as well as in the bulk, as previously discussed in Sections 3.1.3 and 3.1.4. The XPS survey spectra show that La(3d) peaks were found at ~834.2 eV with a La/Al ratio of 0.091 indicating La is in the dispersed phase [17].

3.2. Catalyst activity: bench-scale

The performance of the catalyst using standard diesel as feedstock, at a feed temperature of 650 °C, at three operating conditions: $H_2O/C = 2.5$, $O_2/C = 0.49$; $H_2O/C = 3.0$, $O_2/C = 0.49$; and $H_2O/C = 3.0$ are presented in Table 5. The results presented show that the catalyst with the composition $Rh_{3.0}Ce_{10}La_{10}/\delta$-$Al_2O_3$ is sufficient to obtain complete diesel conversion for all three conditions.

At $H_2O/C = 2.5$, $O_2/C = 0.49$ a high S_{CO_2} (CO_2 selectivity parameter expressed as $CO_2/(CO_2 + CO)$) and H_2 production of 53% and 36 vol%, respectively, are established. These activity results have been reported in a previous study where it was also found that the amount of reducible rhodium oxides as well as the introduction of ceria and lanthana in the delta alumina support had a positive effect on the S_{CO_2} and H_2 formation [6].

At $H_2O/C = 3.0$, $O_2/C = 0.49$ a lower CO content was present in the product gas composition; as a result the S_{CO_2} was increased by 5%. Furthermore, the ethylene formation was reduced from approximately 350 to 300 ppm. These results are in line with what has been presented in the literature [18–22]. The reduction of the concentration of these gas products in the reformate are often prioritized in diesel reforming. For instance, it is well-known that higher levels of CO require extensive CO-clean up, e.g. in a PEFC system. Most problems stem from the CO poisoning effect on the fuel cell itself, as CO is an antagonist to H_2 in the anode reaction and thus can easily adsorb on the electrode, which is often Pt-coated [23]. As for ethylene, it is a well-known coke precursor which can often lead to deactivation of the reforming catalysts due to carbon deposition on the active metal sites [18–22]. Interestingly, looking back at the results in Table 5 at $H_2O/C = 3.0$, $O_2/C = 0.49$ the H_2 formation was not increased. On the contrary H_2 was reduced from 36 to 33 vol%. This trend in the data is unclear; a possible explanation could be the dilution effect caused by the excess of steam in the system [1].

Table 5
Bench-scale results for ATR of a standard diesel fuel (S ~ 6 ppm, C/H ~ 6.43) over catalyst $Rh_{3.0}Ce_{10}La_{10}/\delta$-$Al_2O_3$ at various ATR and SR conditions.

	$H_2O/C \sim 2.5$ $O_2/C \sim 0.49$	$H_2O/C \sim 3.0$ $O_2/C \sim 0.49$	$H_2O/C \sim 3.0$ $O_2/C \sim 0$
X_{diesel} (%)	99.9	99.8	99.8
S_{CO_2} (%)	53	58	39
H_2 (vol%)	36	33	48
CH_4 (ppm)	205	401	3000
C_2H_4 (ppm)	346	305	490

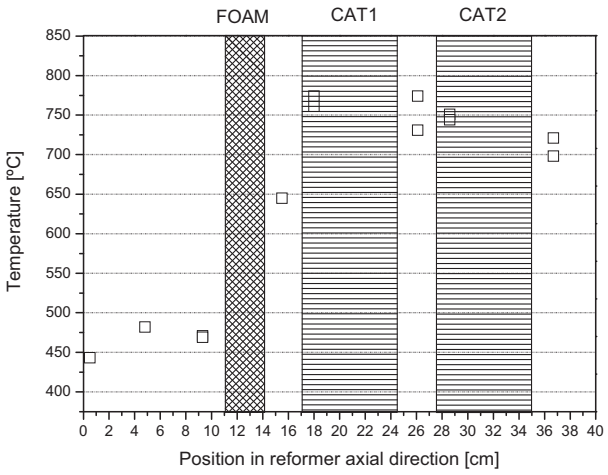

Fig. 3. Full-scale results. Axial temperature measurements over reactor length using diesel MK1 for ATR over catalyst CAT1 and CAT2 both containing the same washcoat composition: $Rh_{3.0}Ce_{10}La_{10}/\delta$-$Al_2O_3$. Operating parameters employed were $H_2O/C = 2.5$, $O_2/C = 0.49$ ($\lambda = 0.33$), GHSV = 10,800 h^{-1} and $P = 1$ atm. FOAM = inert zirconia-treated alumina foam. Detailed information concerning the thermocouple set-up can be found elsewhere [5].

At the final operating condition the oxygen supply was cut off to detect differences in catalyst activity at a ratio of $H_2O/C \sim 3.0$. As expected, the hydrogen generation was greatly improved, reaching a final concentration of 48 vol%. In general, it is well-known that endothermic SR operation favors hydrogen formation [22,24]. Interestingly the S_{CO_2} was reduced to 39%. Also, the methane formation was found to increase 10-fold. Methanation reactions are promoted under SR operation perhaps as a result of the higher hydrogen yield.

3.3. ATR of diesel MK1: full scale

According to Rostrup-Nielsen and Højlund Nielsen [21] activity results acquired from simulations of industrial operation on a bench-scale reactor can be misleading. For instance, at low mass flows, film diffusion restrictions may play a role, which can result in much lower reactant concentrations on the catalyst surface than those experienced in the industrial-sized reactor. Also, deactivation mechanisms such as β deactivation for methanation may not be revealed. Furthermore, in this study, the bench reactor was temperature controlled, whereas the full scale reactor operates more or less adiabatically. Hence, temperature effects on diesel reforming can vary in both cases. Thus, it is recommended to repeat the same experiments at full scale for verification of the activity results. In this study, the temperature measurements at steady state during ATR of diesel MK1 at full scale are presented in Fig. 3. Two catalysts, CAT1 and CAT2, both containing the same washcoat $Rh_{3.0}Ce_{10}La_{10}/\delta$-$Al_2O_3$ were put in the reactor and tested at full-scale. Figs. 4–6 and Table 6 show results obtained at different oxygen-to-carbon and steam-to-carbon ratios.

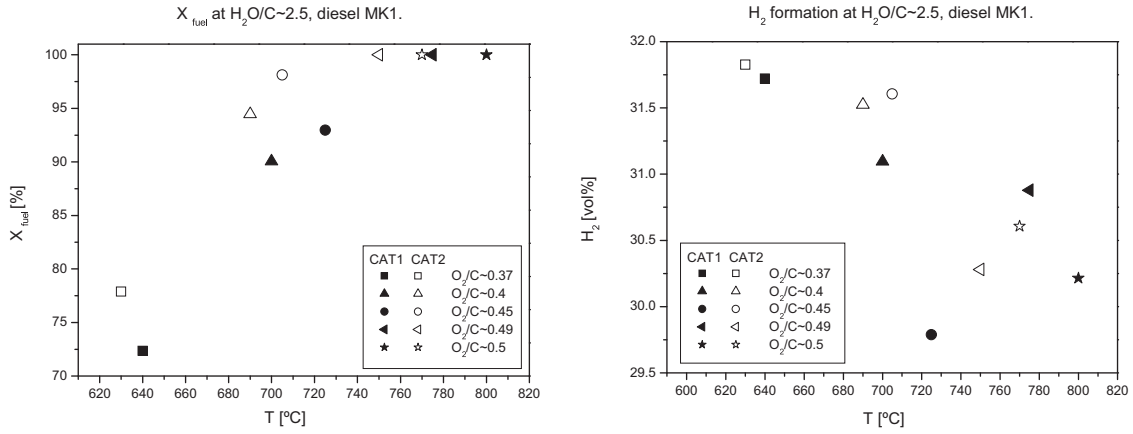

Fig. 4. Full-scale results. The effect of oxygen-to-carbon ratio on diesel MK1. The *y*-axis shows the fuel conversion and hydrogen generation that were measured for both catalysts in the reactor at constant $H_2O/C \sim 2.5$. Filled symbols represent results obtained with CAT1. Unfilled symbols represent CAT2. Both catalysts contain the same washcoat composition: $Rh_{3.0}Ce_{10}La_{10}/\delta\text{-}Al_2O_3$. The x-axis shows the average in-situ temperature of the catalysts measured at reactor $l = 180$ and 290 mm, respectively (see Fig. 3).

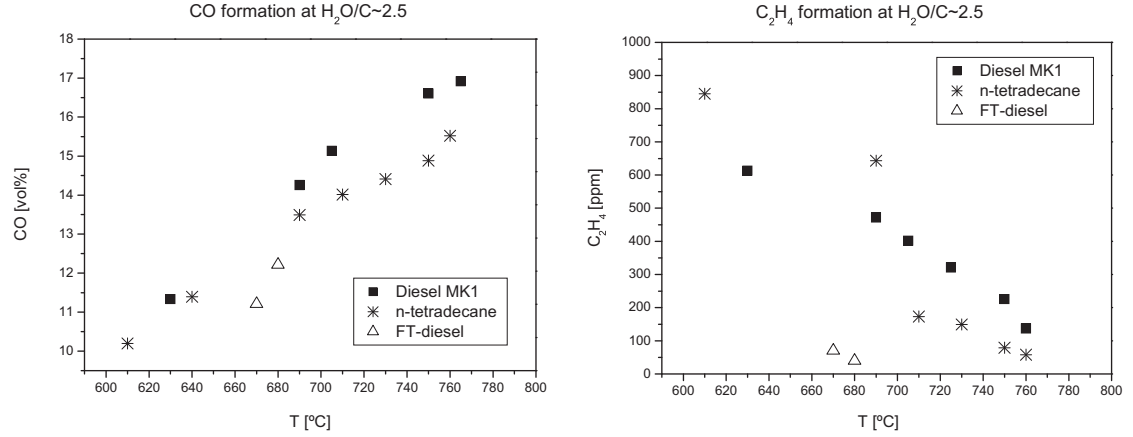

Fig. 5. Full-scale results. The effect of oxygen-to-carbon ratio on CO and C_2H_4 formation. The results were obtained from ATR of diesel MK1, *n*-tetradecane and FT-diesel at constant $H_2O/C \sim 2.5$. The O_2/C ratios where varied to generate average in-situ temperatures in the range of 600–800 °C for CAT2, measured at reactor $l = 290$ mm (see Fig. 3). The tested ranges of the O_2/C ratios are given in Table 2. The gases were analyzed and collected from the outlet of CAT2.

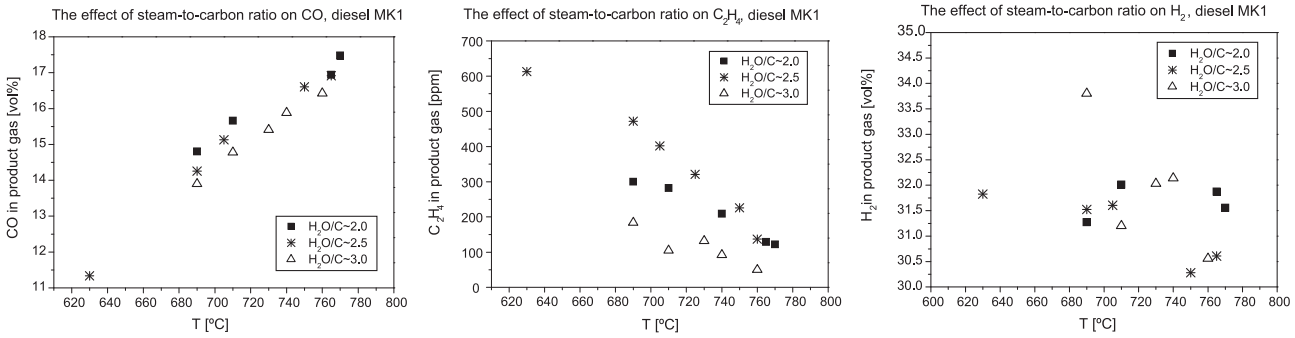

Fig. 6. Full-scale results. The effect of steam-to-carbon ratio on CO, C_2H_4 and H_2 formation. The following results were obtained for ATR of diesel MK1. The H_2O/C ratios tested were 2.0/2.5/3.0. The O_2/C ratios where varied to generate in situ temperatures in the range of 600–800 °C for CAT2 measured at reactor $l = 290$ mm (see Fig. 3). The tested ranges of the O_2/C ratios are given in Table 2. The gases were analyzed and collected from the outlet of CAT2.

Table 6
Full-scale results for ATR of *n*-tetradecane, low-sulfur and FT diesel over catalyst $Rh_{3.0}Ce_{10}La_{10}/\delta\text{-}Al_2O_3$ at constant $H_2O/C \sim 2.5$. The analyzed gas samples were collected from the outlet of CAT2. The average in situ temperature of the catalyst, T_{CAT2}, presented in the table was measured at reactor $l = 290$ mm (see Fig. 3).

	MK1			$C_{14}H_{30}$			FT
	$O_2/C \sim 0.37$	$O_2/C \sim 0.45$	$O_2/C \sim 0.49$	$O_2/C \sim 0.42$	$O_2/C \sim 0.47$	$O_2/C \sim 0.5$	$O_2/C \sim 0.4$
T_{CAT2} (°C)	~650	~700	~750	~650	~700	~750	~700
X_{fuel} (%)	78	98	100	75	97	100	90
S_{CO_2} (%)	48	35	30	44	37	33	51
H_2 (vol%)	31.8	31.6	30.3	32.0	30.3	29.9	32.8
CH_4 (ppm)	4010	4786	4773	3999	10,789	8573	2236

3.3.1. Steady state operation

Fig. 3 shows the temperature profile for diesel MK1 at steady state ($H_2O/C = 2.5$, $O_2/C = 0.49$). This profile is typical for ATR as it displays an initial maximum followed by a decrease of the temperature points measured in the axial direction in the catalytic zone (distance between the front of CAT1 and the back of CAT2). The initial increase of the average temperature noted inside the first catalyst (~770 °C) is believed to be the result of exothermic partial oxidation reactions, see Eq. (2). The decreases noted in the average outlet temperatures of both catalysts, ~750 and 700 °C, measured at reactor $l = 260$ and 370 mm, respectively, indicates that subsequent endothermic steam reforming reactions, see Eq. (3), are taking place along the reactor length. The same trend in major reaction sequences for ATR was seen in the FTIR and GC analyses of the product gases collected from the outlets of both catalysts. In general, all analyses showed that all oxygen was consumed after the first catalyst, CAT1. Furthermore, the highest hydrogen concentrations were found in the outlets from CAT2, see Fig. 4. Similar results have been demonstrated in previous studies using both commercial and in-house made catalysts for diesel MK1 [5,6]. A more detailed discussion regarding possible trends in the product gas distribution is given in the following section.

Partial oxidation (PO)

$$C_xH_y + \frac{x}{2}(O_2 + 3.76N_2) \rightarrow xCO + \frac{y}{2}H_2 + \frac{x}{2}3.76N_2 \quad (\Delta H^\circ < 0 \ \text{kJ/mol}) \tag{2}$$

Steam reforming (SR)

$$C_xH_y + xH_2O \rightarrow xCO + \left(x + \frac{1}{2}y\right)H_2 \quad (\Delta H^\circ > 0 \ \text{kJ/mol}) \tag{3}$$

3.3.2. The effect of oxygen-to-carbon ratio

Fig. 4 shows the fuel conversion for diesel MK1 as a function of the average gas temperature measured in situ for both catalysts at reactor $l = 180$ and 290 mm, respectively. In this experiment the steam-to-carbon ratio was kept constant at 2.5, while the oxygen-to-carbon ratio was varied between 0.37 and 0.5 to establish average in situ temperatures in the range of 600–800 °C. As seen in Fig. 4, the fuel conversion was improved with an increase in temperature, O_2/C ratio and catalyst volume. Also, the conversion was higher at lower temperatures for the second catalyst. This is due to the occurrence of steam reforming reactions, as previously discussed in Section 3.3.1 and seen in Fig. 3. Also, a complete conversion of diesel MK1 was achieved at a temperature of ~750 °C, which is achieved with $O_2/C \sim 0.49$. It should be emphasized that the optimum operating parameter for O_2/C is unique for each reformer system. For instance, other research groups have reported lower oxygen-to-carbon, in the vicinity of ~0.2 to 0.3 [25,26] in order to reach the same temperature range. In this study the steam and air feed is only pre-heated to 300 °C and thus a greater degree of oxidation of the fuel is required to provide heat required to vaporize the fuel and reach the in situ reactor temperatures of 700–750 °C. Other groups either pre-heat the feed gases to temperatures in excess of 700 °C [25] or use the combustion of off-gases from the fuel cell to provide additional heat to the reforming reactor [26] to achieve high fuel conversion.

Table 6 shows the FTIR and GC analyses made from samples collected from the outlets from CAT2. As seen in Table 6, the increase in the oxygen-to-carbon ratio had a clear impact on the product gas distribution. For instance, S_{CO_2} decreased with higher oxygen-to-carbon ratio. The S_{CO_2} is 48% and 30% at $O_2/C \sim 0.37$ and 0.49, respectively. Furthermore, the hydrogen content in the reformate was also affected negatively as it decreased from approximately 32 to 30 vol% (see also Fig 4). There are several explanations available to describe the negative S_{CO_2} and H_2 trends. In general, an increase in oxygen-to-carbon ratio promotes oxidation reactions, in particular the CO formation as seen in Fig. 5. Furthermore, it pushes the ATR process closer towards the operating range for partial oxidation which, according to thermodynamics, lowers the amount of hydrogen produced, see Eqs. (2) and (3). In addition, more nitrogen enters the system, causing dilution of the product gas [1]. Regarding methane formation, as seen in Table 6, it increases as more diesel is converted. Interestingly, the methane formation reached a maximum at $O_2/C \sim 0.45$ before leveling off at higher ratios. Another interesting result is the reduction of ethylene, which can be seen in Fig. 5. In this figure, the highest ethylene concentration, close to 600 ppm, was found at 630 °C. Furthermore, ethylene was reduced to almost zero at temperatures in the vicinity of 800 °C. This result is in line with what has been reported by others [18,27]. In general, a minor extra addition of oxygen or air in the feedstock is beneficial as it can suppress ethylene formation [19–21]. It can also assist in removing the surface carbon residues by oxidation at temperatures above 500 °C [19–21]. However, it should also be noted that the removal of carbon species through oxygen can also cause damage to the catalyst as the surface temperature will be significantly elevated, leading to possible losses of active particles from the support [19–22]. This phenomenon was clearly noted in a previous study, where losses of Rh were observed, particularly at the front part of the catalyst where oxidation reactions were believed to predominate [6]. The role of the catalyst composition, $Rh_{3.0}Ce_{10}La_{10}/\delta\text{-}Al_2O_3$, for ATR with regard to ethylene formation has been discussed in that study where it was noted that the introduction of Ce and La in the support was found to reduce coke and ethylene formation. Also, XPS analysis showed an increase of CeO_2 formation in the washcoat in the front part of an aged catalyst where oxidation reactions reign [6].

3.3.3. The effect of steam-to-carbon ratio

The effect of steam-to-carbon ratio can be seen in Fig. 6. As seen in the figure, the CO and C_2H_4 formations are reduced with higher steam-to-carbon ratio. The average reduction for CO at each sampling point was ~1 vol% as H_2O/C was increased from 2 to 3 in the temperature range 600–800 °C. The corresponding value for C_2H_4 was ~250 ppm. Hence, these results confirm the activity measurements obtained from the bench-scale experiments as the same declining CO and C_2H_4 trends were noted (see Table 5).

Regarding hydrogen, the highest concentration, ~33.8 vol%, was found at a ratio of $H_2O/C \sim 3.0$ at 690 °C, as seen in Fig. 6. The hydrogen formation was found to decrease with higher temperatures for most ratios tested except for $H_2O/C \sim 2.0$. Also, it was difficult to distinguish just by observing the scattered data points in Fig. 6, if an increase in steam-to-carbon ratio affected the hydrogen generation. In order to better depict possible trends, total average values were calculated and implemented instead. The average hydrogen concentrations for each ratio are the following: ($H_2O/C \sim 2.0$) 31.7 vol%; ($H_2O/C \sim 2.5$) 31.2 vol%; and ($H_2O/C \sim 3.0$) 31.9 vol%. Again, small differences are noted in hydrogen productivity. However, based on these results the highest average hydrogen concentration was noted for the highest steam-to-carbon ratio. This result is in line with what has been reported in the literature [26,28,29]. In general, higher steam-to-carbon ratios push the ATR process closer towards the operating range for endothermic steam reforming, which favors hydrogen formation. Also, in this study, the steam reforming effect was noted in the temperature measurements. At any value of O_2/C, an increase of H_2O/C, while maintaining all other operating parameters constant, resulted in lower reaction temperatures.

3.4. ATR of n-tetradecane ($C_{14}H_{30}$): full-scale

The results for ATR of *n*-tetradecane are discussed in Sections 3.4.1 and 3.4.2.

3.4.1. The effect of oxygen-to-carbon ratio

For ATR of *n*-tetradecane, the reactant mixture was ignited at 290 °C, which is ~10 °C lower than reported for diesel MK1 [5,6]. Furthermore, the temperature profile and the fuel conversion trend were found to be similar to those of diesel MK1. For instance, as seen in Table 6, the same level of catalyst temperature was reached, $T_{CAT2} \sim 750$ °C, in order to achieve complete conversion of *n*-tetradecane.

The effect of oxygen-to-carbon ratio can be seen in Fig. 5. As seen in the figure, the CO and C_2H_4 plots follow the same trends as noted for diesel MK1. However, the CO concentration for *n*-tetradecane is significantly lower, by ~1 vol% for each sampling point, compared to diesel MK1. The concentration of C_2H_4 is also considerably lower, ~250 ppm. This is a clear example of the fuel–feedstock composition effect on the reaction mechanism for autothermal reforming. For instance, it is well known that the amount of aromatics and sulfur present in the fuel is an important factor, as they are known to promote the formation of coke precursors, e.g. ethylene [30,31]. As seen in Table 2, diesel MK1 contains ~5 vol% aromatics and ~10 ppm S. Furthermore, these fuel ingredients can also promote CO formation, as previously described and seen in Fig. 5. This latter phenomenon was clearly noted in a previous study where ATR of E85 (85 vol% ethanol, 15 vol% gasoline) and pure ethanol were performed over wt% $Rh/\gamma\text{-}Al_2O_3$. The higher aromatic and sulfur content present in E85, ~8 vol% and ~10 ppm, respectively, resulted in a significantly higher CO formation, ~4 vol% than for neat ethanol [32].

For *n*-tetradecane, as seen in Table 6, higher oxygen-to-carbon ratios were needed in order to reach the same catalyst temperatures as for diesel MK1. For instance, the O_2/C was ~0.42 in comparison to ~0.37 for diesel MK1, to achieve a catalyst temperature of $T_{CAT2} \sim 650$ °C. Again, this phenomenon can be attributed to fuel composition, in particular the aromatics. For instance, in an ATR study by Flytzani-Stephanopoulos and Voecks [30], it was found that the addition of benzene into *n*-tetradecane promoted exothermic reactions. As a result, the reaction temperature for a benzene–tetradecane mixture was higher than the corresponding temperature for pure *n*-tetradecane. Hence, higher oxygen-to-carbon ratios were needed in order to convert pure tetradecane.

In this study, the hydrogen concentration obtained from *n*-tetradecane was similar to that measured for diesel MK1, as seen in Table 6. This indicates that the feedstock composition of the employed fuels had only a minor effect on the hydrogen generation. As for methane, higher concentrations were found present in the outlet streams of the catalysts from *n*-tetradecane reforming. Also, the same methane trend was noted as for diesel MK1 with a methane maximum, ~10,800 ppm, registered at $T_{CAT2} \sim 700$ °C ($O_2/C \sim 0.47$) followed by an decrease, ~8600 ppm, at 750 °C ($O_2/C \sim 0.5$).

The role of the catalyst composition, $Rh_{3.0}Ce_{10}La_{10}/\delta\text{-}Al_2O_3$, for ATR with regard to the fuel properties of diesel, e.g. aromatics and sulfur, has not been investigated in this study. However, it has been reported that Rh has a higher resistance towards coke deposition and sulfur poisoning than other noble metals such as Pt and Pd [25,31].

3.4.2. The effect of steam-to-carbon ratio

The effect of steam-to-carbon ratio on *n*-tetradecane had a similar impact on the product gas distribution as the ones noted for diesel MK1. The CO and C_2H_4 formations were reduced by ~0.5 vol% and ~150 ppm, respectively, as H_2O/C was increased from 2 to 3.0. Also higher concentrations of H_2 were observed. The average hydrogen concentrations for each ratio are the following: ($H_2O/C \sim 2.0$) 31.7 vol%; ($H_2O/C \sim 2.5$) 31.2 vol%; and ($H_2O/C \sim 3.2$) 32.2 vol%. These results are similar to those reported for diesel MK1, see Section 3.3.3, suggesting once again that the feedstock composition, e.g. aromatics and sulfur, of the employed fuels had a minor effect on hydrogen generation.

3.5. ATR of Fischer–Tropsch diesel: full-scale

The results for ATR of FT-diesel are discussed in Sections 3.5.1 and 3.5.2.

3.5.1. The effect of oxygen-to-carbon ratio

For ATR of FT-diesel, the reactant mixture was ignited at 300 °C, thus the light-off temperature was the same as for diesel MK1. Furthermore, the temperature profile was not different from the ones obtained operating with *n*-tetradecane and diesel MK1.

In this study, approximately after 2 h of steady-state operation, the temperature gradient in the mixing zone was found to slowly increase. Furthermore, a constant increase in both in situ catalyst temperatures was detected. All ATR experiments involving FT-diesel showed the same trend. This problem was also noted in a previous study where ignition of light fractions in the fuel was believed to have caused the temperature gradients [6]. In both studies, the same fuel from the same manufacturer was employed. Hence, one may argue whether the unstable operation noted may be attributed to this particular fuel or to FT-diesel fuel, in general. Nevertheless, owing to problems in maintaining steady state operation with increased time on stream, only the initial gas samples, within the first 2 h of operation, were collected and analyzed in detail. In this case, gas samples were collected from the outlets of CAT2 at the following reaction conditions: $H_2O/C \sim 2.5$ (constant), and $O_2/C \sim 0.39$ and 0.40, latter resulting in a catalyst temperature of $T_{CAT2} \sim 700$ °C. The results can be seen in Fig. 5 and Table 6. As seen in Fig. 5, lower concentrations of CO and C_2H_4 were found in the reformate than for diesel MK1 and *n*-tetradecane in the same temperature region. Also, as seen in Table 6, a higher S_{CO_2} and hydrogen concentration, ~51% and 32.8 vol%, respectively, were noted for FT-diesel. In addition, the methane formation was lower. However, it should be noted that the fuel conversion was lower as a result of the lower O_2/C ratio implemented. Judging from these results, FT-diesel shows the same overall trend in the product gas distribution for *n*-tetradecane than for diesel MK1. Hence, these results may be ascribed to the fuel composition effect, e.g. since a higher quantity of paraffins and lower amounts of aromatics and sulfur are present in *n*-tetradecane as well as in FT-diesel, than in diesel MK1. However, further analysis and more samples must be collected over a longer period of steady-state operation, in particular for FT-diesel reforming, in order to confirm these trends.

3.5.2. The effect of steam-to-carbon ratio

As previously described in Section 3.5.1, owing to problems in maintaining steady state operation with increased time on stream, few gas samples were collected and analyzed in detail and only at $H_2O/C \sim 3.2$. Hence, due to the limited data, it was difficult to distinguish any clear trends, e.g. in the product gas distribution data, owing to the effect of the steam-to-carbon ratio.

3.6. Final remarks

For all fuels tested in the full-scale experiments, no catalyst deactivation, e.g. carbon deposition and sulfur poisoning were noted during the ongoing experiments, during shutdown of the reactor and during visual examination of the catalysts. The total time on stream for each fuel tested was approximately 40 h. The

same activity results were acquired when the same reaction conditions were repeated.

4. Conclusions

This study demonstrates the use of rhodium-based monolithic catalysts for onboard reforming of diesel fuels. The results provide a deeper understanding regarding possible reaction mechanisms occurring during ATR of diesel that can be correlated with the catalyst and fuel properties. In this study, a catalyst with the composition $Rh_{3.0}Ce_{10}La_{10}/\delta$-$Al_2O_3$ was tested both in bench and in full-scale reactors. The diesel surrogate *n*-tetradecane, and commercial low-sulfur and FT diesel fuels were used to detect differences in catalyst activity during industrial-scale operation. All results were reproducible and steady-state conditions were established for all experiments. Fresh powder samples of the catalyst were characterized using XRD, N_2-BET, H_2 chemisorption, H_2-TPR and XPS analyses. The conclusions listed below can be made.

The characterization results were:

- The BET analysis showed that the surface area, pore volume and pore diameter are reduced when the noble metal and the promoters are impregnated on the support.
- The H_2-chemisorption analysis showed that high rhodium dispersion, ~42%, was obtained for the alumina-supported catalyst.
- The diffractograms from the XRD analysis showed patterns ascribed to δ-alumina to be present. Finely dispersed fluorite-structured CeO_2 was also found present in the bulk.
- The H_2-TPR measurements showed the presence of rhodium bulk oxides and cerium oxides.
- The XPS analysis showed rhodium oxides, ceria in the form of CeO_2 and lanthana in the dispersed phase all to be present on the surface of the catalyst.

The catalyst activity results from the bench-scale experiments show that:

- The choice of reforming process had a clear effect on the catalyst performance. A clear difference in catalyst activity, e.g. in terms of hydrogen production, was noted between ATR and SR operation.

The catalyst activity results from the full-scale experiments are:

- The temperature measurements and analyzed product gases established that the sequence of the main reactions taking place for ATR of diesel were primarily initial oxidation followed by steam reforming.
- The choice of H_2O/C and O_2/C ratios had a clear effect on the product gas distribution. In general, increasing the H_2O/C ratio increased the H_2 and decreased CO formation, while increasing the O_2/C ratio decreased the H_2 and CO production.
- The result from the full-scale operation could be correlated with the results from the bench-scale experiments. For instance, similar declining carbon monoxide and ethylene trends were noted, in both cases, with increasing H_2O/C.
- Fuel properties have a clear effect on the catalyst performance. The fuels containing less aromatics and sulfur were found to result in less carbon monoxide and ethylene formation.

Acknowledgements

The Foundation for Strategic Environmental Research (MISTRA) and the Foundation of Strategic Research (SSF) are gratefully acknowledged for financial support. Thanks also to Corning Inc. for supplying cordierite substrates and to Sasol Germany GmbH for providing the alumina.

References

[1] M. Nilsson, Hydrogen generation for fuel cells in auxiliary power systems, PhD Thesis, KTH, Department of Chemical Engineering and Technology, TRITA-CHE Report 2009:7, 2009, ISBN 978-91-7415-245-6.
[2] R. Lanza, E. Eriksson, L.J. Pettersson, Catal. Today 147 (2009) S279–S284.
[3] A. Abu-Jrai, A. Tsolakis, K. Theinnoi, A. Megaritis, S.E. Golunski, Chem. Eng. J. 141 (2008) 290–297.
[4] B.D. Gould, X. Chen, J.W. Schwank, J. Catal. 250 (2007) 209–221.
[5] X. Karatzas, M. Nilsson, J. Dawody, B. Lindström, L.J. Pettersson, Chem. Eng. J. 156 (2010) 366–379.
[6] X. Karatzas, J. Dawody, A. Grant, E. Elm Svensson, L.J. Pettersson, Appl. Catal. B, submitted for publication. doi:10.1016/j.apcatb.2010.09.027.
[7] Dieselnet, www.dieselnet.com, last visited 01.05.2010.
[8] The Swedish Petroleum Institute, SPI, www.spi.se, last visited 01.06.2010.
[9] FramtidsBränslen Sverige AB, www.framtidsbranslen.se, last visited 01.05.2010.
[10] W.G. Dukek, in: J.I. Kroschwitz, M. Howe-Grant (Eds.), Kirk-Othmer Encyclopedia of Chemical Technology, 4th ed., Wiley-Interscience Publication, New York, 1992.
[11] I. Pettiti, S. Colonna, S.D. Rossi, M. Faticanti, G. Minelli, P. Porta, Phys. Chem. Chem. Phys. 6 (2004) 1350–1358.
[12] S. Damyanova, J.M.C. Bueno, Appl. Catal. A 253 (2003) 135–150.
[13] C. Hwang, C. Yeh, Q. Zhu, Catal. Today 51 (1999) 93–101.
[14] H.C. Yao, Y.F. Yu Yao, J. Catal. 86 (1984) 254–265.
[15] R. Polvinen, M. Vippola, M. Valden, T. Lepistö, A. Suopanki, M. Härkönen, J. Catal. 226 (2004) 372–381.
[16] P. Burroughs, A. Hamnett, A.F. Orchard, G. Thomton, J. Chem. Soc., Dalton Trans. 17 (1976) 1686–1698.
[17] L.P. Haack, J.E. deVries, K. Otto, M.S. Chattha, Appl. Catal. A 82 (1992) 199–214.
[18] S. Yoon, I. Kang, J. Bae, Int. J. Hydrogen Energy 22 (2008) 4780–4788.
[19] J.R. Rostrup-Nielsen, T.S. Christensen, I. Dybkjaer, Stud. Surf. Sci. Catal. 113 (1998) 81–95.
[20] J.R. Rostrup-Nielsen, in: J.R. Anderson, M. Boudart (Eds.), Catalysis, Science and Technology, vol. 5, Springer-Verlag, Berlin, 1984, Chapter 1.
[21] J.R. Rostrup-Nielsen, P.E. Højlund Nielsen, in: J. Oudar, H. Wise (Eds.), Deactivation and Poisoning of Catalysts, Marcel Dekker, Inc., New York, 1985, Chapter 7.
[22] G. Kolb, Fuel Processing, Wiley-VCH Verlag GmbH & Co. KGaA, Weinheim, 2008.
[23] X. Cheng, Z. Shi, N. Glass, L. Zhang, J. Zhang, D. Song, Z.S. Liu, H. Wang, J. Shen, J. Power Sources 165 (2007) 739–756.
[24] S. Specchia, A. Cutillo, G. Saracco, V. Specchia, Ind. Eng. Chem. Res. 45 (2006) 5298–5307.
[25] R.K. Kaila, A. Gutiérrez, A.O.I. Krause, Appl. Catal. B 84 (2008) 324–331.
[26] D. Liu, M. Krumpelt, Int. J. Appl. Ceram. Technol. 2 (2005) 301–307.
[27] M. O'Connell, G. Kolb, K.P. Schelhaas, J. Shuerer, D. Tiemann, A. Ziogas, V. Hessel, Int. J. Hydrogen Energy 34 (2009) 6290–6303.
[28] D. Liu, T.D. Kaun, H. Liao, S. Ahmed, Int. J. Hydrogen Energy 29 (2004) 1035–1046.
[29] D. Shekhawat, T.H. Gardner, D.A. Berry, J.J. Spivey, in: J.J. Spivey (Ed.), Catalysis, vol. 19, Royal Society of Chemistry, London, 2006, Chapter 6.
[30] M. Flytzani-Stephanopoulos, G.E. Voecks, Int. J. Hydrogen Energy 8 (1983) 539–548.
[31] A.C. McCoy, M.J. Duran, A.M. Azad, S. Chattopadhyay, M.A. Abraham, Energ. Fuel. 21 (2007) 3513–3519.
[32] M. Nilsson, X. Karatzas, B. Lindström, L.J. Pettersson, Chem. Eng. J. 142 (2008) 309–317.